Continental Shelf Research 137 (2017) 56–71

Contents lists available at ScienceDirect

Continental Shelf Research

journal homepage: www.elsevier.com/locate/csr

Research papers

Sea-level rise impacts on the tides of the European Shelf

Déborah Idier[a,*], François Paris[a], Gonéri Le Cozannet[a], Faiza Boulahya[a], Franck Dumas[b,1]

[a] BRGM, 3, avenue C. Guillemin, 45060 Orléans cedex 2, France
[b] IFREMER, Centre de Brest BP 70, 29280 Plouzané, France

ARTICLE INFO

Keywords:
Tide
Sea-level rise
Tidal component
Climate change
European Shelf
Resonance

ABSTRACT

Sea-level rise (SLR) can modify not only total water levels, but also tidal dynamics. Several studies have investigated the effects of SLR on the tides of the western European continental shelf (mainly the M2 component). We further investigate this issue using a modelling-based approach, considering uniform SLR scenarios from −0.25 m to +10 m above present-day sea level. Assuming that coastal defenses are constructed along present-day shorelines, the patterns of change in high tide levels (annual maximum water level) are spatially similar, regardless of the magnitude of sea-level rise (i.e., the sign of the change remains the same, regardless of the SLR scenario) over most of the area (70%). Notable increases in high tide levels occur especially in the northern Irish Sea, the southern part of the North Sea and the German Bight, and decreases occur mainly in the western English Channel. These changes are generally proportional to SLR, as long as SLR remains smaller than 2 m. Depending on the location, they can account for +/−15% of regional SLR. High tide levels and the M2 component exhibit slightly different patterns. Analysis of the 12 largest tidal components highlights the need to take into account at least the M2, S2, N2, M4, MS4 and MN4 components when investigating the effects of SLR on tides. Changes in high tide levels are much less proportional to SLR when flooding is allowed, in particular in the German Bight. However, some areas (e.g., the English Channel) are not very sensitive to this option, meaning that the effects of SLR would be predictable in these areas, even if future coastal defense strategies are ignored. Physically, SLR-induced tidal changes result from the competition between reductions in bed friction damping, changes in resonance properties and increased reflection at the coast, i.e., local and non-local processes. A preliminary estimate of tidal changes by 2100 under a plausible non-uniform SLR scenario (using the RCP4.5 scenario) is provided. Though the changes display similar patterns, the high water levels appear to be sensitive to the non-uniformity of SLR.

1. Introduction

Coastal plains are a prime example of risk-prone areas. Coastal flooding risks are expected to increase, due to both population growth in coastal areas and a greater likelihood of coastal flooding, which is a response to climate change and the resulting rise in mean sea-level (Hinkel et al., 2013; Wong et al., 2014). In theory, sea-level rise (SLR) has a direct effect on total instantaneous water levels, as well as indirect effects on tides and storm surges (e.g., Weisse et al., 2012). These indirect effects can be considered negligible in deep water, but may become significant in shallow-water areas, where non-linear interaction processes are generated (Pugh, 1987). Arns et al. (2015) found that an SLR of +0.54 m induces an increase in high water levels (in addition to SLR) that exceeds 10 cm in the shallow-water areas of the Wadden Sea, and also that the water level changes in the German Bight are caused by non-linear and spatially not coherent changes in the tidal constituents. It is therefore worthwhile to better understand and map the effects of SLR on tides in shallow-water areas such as the western European continental shelf.

As discussed by Pugh (1987), this shelf is subject to the following tidal dynamics. The Atlantic semi-diurnal Kelvin wave propagates from south to north. Energy is transmitted to the Celtic Sea and the English Channel, where it partly leaks into the North Sea and to the North Sea by diffraction around the north of Scotland (Fig. 1b). The English Channel and the Irish Sea respond similarly to the incoming wave from the Celtic Sea (a tidal wave takes about seven hours to travel from the shelf edge to the entrance of the Irish Sea and the Dover Strait). In addition to the presence of 6 amphidromic points (3 complete and 3 degenerate), several areas are close to resonance (e.g., Celtic Sea and Bristol Channel). The first question that arises is, “What is the influence of SLR on this complex set of tidal dynamics?”

Both at the global scale and within the western European shelf area,

* Corresponding author.
E-mail address: d.idier@brgm.fr (D. Idier).
[1] Presently at SHOM, 13, rue du Chatellier BP 30316, 29603 Brest, France.

http://dx.doi.org/10.1016/j.csr.2017.01.007
Received 15 April 2015; Received in revised form 12 January 2017; Accepted 16 January 2017
Available online 17 January 2017

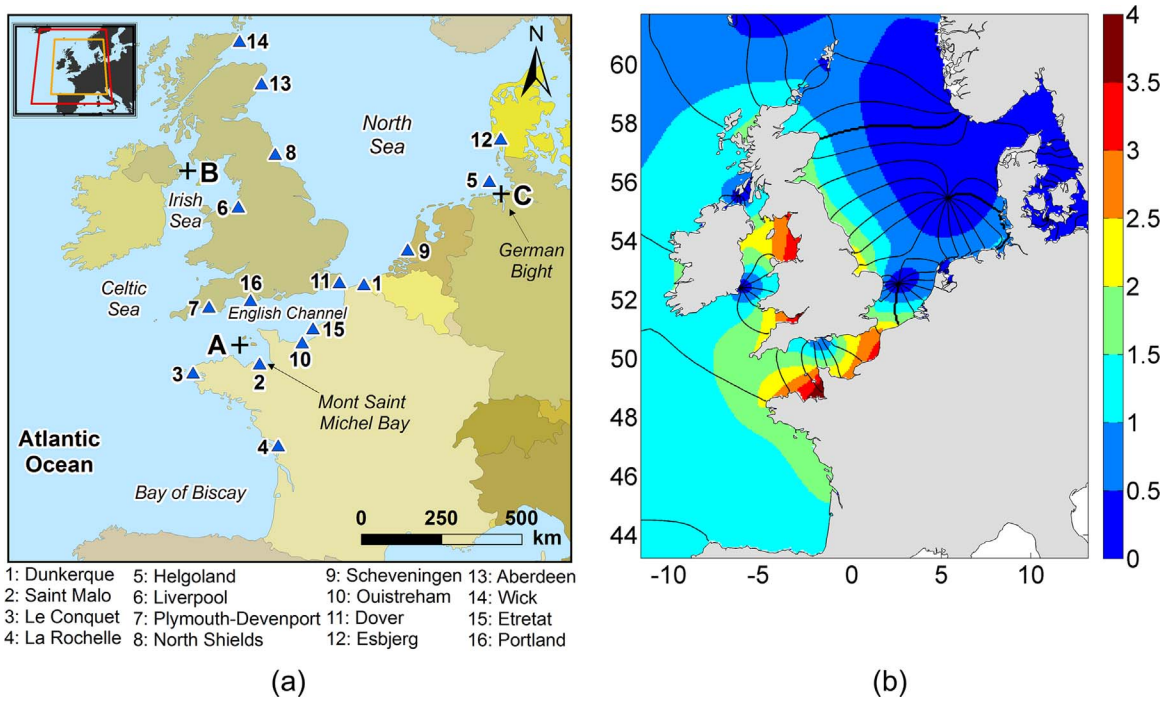

Fig. 1. (a) Computational domain of the hydrodynamic model and the locations of tide gauges used to validate the model; (b) Co-tidal chart for the modeled M2 component. Thick line indicates the 0° phase, and dotted contours indicate the phase every 30°. Tide rotation around amphidromic points is counter-clockwise.

tide gauge analyses over the last century show changes in the characteristics of primary tidal components M2, S2, K1 and O1 (Woodworth, 2010). As highlighted by Woodworth (2010) and Pickering et al. (2012), many phenomena can contribute to these changes (including local phenomena such as dredging, harbor construction, resonance changes and meteorological effects, in addition to SLR). To isolate the influence of SLR on European shelf tides, many studies have used a modelling approach (e.g. de Ronde, 1989). The most recent comparable studies, i.e., Pickering et al. (2012), Ward et al. (2012), and Pelling et al. (2013, 2014) investigate the effects of uniform SLR scenarios. These studies use two main coastal defense scenarios. (1) In one of these scenarios, the grid cells located inland can be flooded (hereafter called the “flood” scenario). (2) In the other scenario, they cannot, meaning that the computational domain stops at the shoreline, and therefore that the coastal defenses are assumed to be infinitely high (hereafter called the “no flood” scenario). Indeed, tides alone can cause flooding in areas such as the Netherlands, so that considering coastal defenses potentially impacts the results of tidal modelling. These recent studies produce consistent results for comparable tests (i.e., using the same SLR scenario and flooding options). For an SLR of +2 m and in a “no flood” case, Pickering et al. (2012) and Pelling et al. (2013) obtain variations in M2 tidal amplitude ranging from −15% to +15% of the SLR. Both studies anticipate increases in M2 amplitudes in the Irish Sea, the southern North Sea, and the eastern English Channel, as well as decreases in M2 amplitudes in the western English Channel and the Celtic Sea. However, the signs and magnitudes of the changes display local discrepancies. For instance, Pickering et al. (2012) obtained an increase in M2 amplitude in the German Bight, whereas Pelling et al. (2013) obtained a decrease. Furthermore, Pickering et al. (2012), who investigated +2 m and +10 m SLR scenarios, conclude that the M2 tidal response is non-linear in the North Sea, whereas Pelling et al. (2013) found that the behavior was (nearly) linear (for SLR ranging from +2 m to +5 m). In these papers, "linear" was used to refer to tidal changes that are proportional to sea-level rise values. As the physical processes behind the SLR-tide interaction are fully non-linear, the term “proportional” is preferred in the present paper.

The above results were obtained for “no flood” scenarios. Pelling et al. (2013) show that tidal changes are sensitive to the coastal flooding option chosen. For instance, for the +2 m SLR scenario and for the “flood” case, they obtain a decrease in M2 amplitude in the Irish Sea (i.e., a trend opposite to that seen in the “no flood” case). For a larger SLR (+5 m), the M2 amplitude increases. Thus, in this area, the spatial patterns of positive and negative changes depend on the magnitude of SLR. Such a dependence of spatial patterns on the value of SLR is also found in the North Sea when flooding is allowed. In the present paper, the term spatial similarity refers to cases in which the sign (plus/minus) of the ratio between tidal changes and sea-level rise is constant at a given location (so that the areas with positive and negative signs remain the same), regardless of the sea-level rise scenario. In this case, the changes are characterized as being spatially similar.

The above modelling studies investigate the influence of uniform SLR either on the M2 or on the M2, S2 and M4 tidal components. The time span covered by the computations was limited to tens of days (a maximum of 30 days in the studies of Ward et al. (2012) and Pelling et al. (2013)), restricting the investigation of additional tidal components, as well as the influence on the highest and lowest tide levels that would be reached during a longer time span. As suggested by Pickering et al. (2012), “For an accurate harmonic analysis of all significant constituents a longer model run (1 year) would be required”. In addition, although the proportionality between the M2 component and SLR has been discussed (e.g., Pelling et al., 2013), no studies have systematically quantified the spatial similarity and proportionality of the tidal response (e.g., the M2 amplitude and high tide level) with respect to sea-level rise on a scale of several kilometers over the entire western European continental shelf.

The present paper investigates the effects of SLR on the tides of the western European continental shelf by addressing the following questions: (Q1) What is the influence of sea-level rise on water levels in terms of spatial similarity, proportionality and the contributions of tidal components? (Q2) What are the main mechanisms at work? (Q3) To what extent are the results affected by allowing or not allowing inland flooding? (Q4) What would be the effect of a non-uniform SLR

that could plausibly occur by 2100?

First, the method is described (Section 2). Then, the effects of SLR on tidal water levels and components are analyzed (Section 3). The possible physical mechanisms producing these changes (e.g., resonance, friction, and reflection) and the effects of allowing inland flooding are analyzed in Section 4. In Section 5, we investigate the effects of a regionally variable SLR scenario, discuss the modelling assumptions, compare our results with those from previous studies and discuss the implications of our conclusions for flooding hazard assessment. Conclusions are drawn in the last section.

2. Methods

2.1. Hydrodynamic model and validation

The selected numerical model is MARS, which is based on the shallow-water equations (Lazure and Dumas, 2008). The computational domain (Fig. 1a, shown as a red box in the inset) is large enough to ensure that sea-level rise has no impact on the tidal components at the open boundaries of the domain. The grid cell size is 2 km (maps showing the results are plotted at a resolution of 6 km). Bed shear stress is computed using a Strickler coefficient of 35 $m^{1/3}\ s^{-1}$, which corresponds to a drag coefficient of 0.0026 for a water depth of 30 m. The 14 main tidal components (Mf, Mm, Msqm, Mtm, O1, P1, Q1, K1, M2, K2, 2N2, N2, S2 and M4) are used to force the tide at the open boundaries, and these components are derived from the FES2004 global tidal model (Lyard et al., 2006). As in the study of Pickering et al. (2012), the direct effect of the tide-generating force is not taken into account (as shown by Gerritsen et al. (1995), the European Shelf is too small and too shallow to respond significantly to such forcing). The bathymetric and topographic data come from the GEBCO database (in deeper areas), bathymetric lidar and echo-sounding measurements (in shallower areas), and also the GTOPO30 data (in inland areas).

In the first part of this study, we consider a “no flood” scenario, which is a realistic assumption for coasts such as the Netherlands (Pickering et al., 2012). However, predicting future coastal defenses in other areas remains highly uncertain. Thus, the influence of uniform coastal defense strategies (“no flood” vs.”flood”) is further discussed in Section 4.

Our model is similar to the one used and validated by Idier et al. (2012) for the English Channel. Here, we complete the validation at a scale covering the entire western European Shelf. First, the comparison of the M2 co-tidal map obtained from our model (Fig. 1b) with those based on measurements (Howarth, 1990) and other modelling experiments (e.g., Pelling and Green, 2014) shows that the six M2 amphidromic systems (of which three are in the North Sea, one is in the English Channel, one is in the Celtic Sea, and one is in the Irish Sea) and the related M2 amplitude and phases are properly reproduced.

Modeled water levels are then compared to tide gauge data from 16 locations (Fig. 1a), over the entire year 2009. Instead of using direct observations, which contain gaps at some sites, we use the continuous data-based tidal predictions provided by SHOM. These predictions are based on tidal component analyses of water level records covering many years. Comparison of the modeled and data-based highest annual tides shows that most of the sites exhibit an error smaller than 5% (shown in blue in Fig. 2a). The largest relative errors are probably related to the 2-km resolution of the model, which is slightly coarse to allow for accurate reproduction of tides at gauges located at sites characterized by complex configurations, as in the cases of tide gauges S4 (which is located in a harbor in front of the 1.8-km-wide channel between La Rochelle and Ré Island), S5 (which is located on Helgoland, which is made up of two islands with widths less than 1 km) and S10 (which is located at the entrance of a river and a channel that is open from time to time). Excluding S4, S5 and S10, the rms error is 0.078 m, and the r^2 value is 0.997. Thus, the model reproduces the overall features of the highest tides quite accurately, though its coarse resolution should be borne in mind when making comparisons with data from particular tide gauge stations.

To complete the validation, we performed a tidal components analysis of both the model results and the data-based tide prediction we used above, covering the entire year 2009. For this analysis, we used the Tidal Toolbox software (provided by LEGOS) and ensured that each component computed with this toolbox (i.e., 93) was effectively present in the data-based tidal prediction. Comparison of the modeled and data-based tidal components (see Fig. 2b for the 5 main components M2, S2, K2, N2 and M4) shows that the quality is comparable to that of similar studies (e.g., Arns et al., 2015).

2.2. Simulations, analyses and sea-level rise scenarios

If there were no change in the tidal dynamics, future water levels induced by SLR and tides could be estimated by adding the SLR to the present tide (ξ). In the following analysis, we investigate the effects of SLR on tides, and more specifically on the highest tide level (ξ_{max}) reached during the simulated year 2009 and on the amplitudes and phases of the tidal components (CST_{amp} and CST_{phase}, respectively, with CST representing the name of the tidal component). The analysis is performed for the area covered by Fig. 1b. We compute ξ_{max}, CST_{amp} and CST_{phase} using the Tidal Toolbox software. We focus on tidal components having amplitudes larger than 10 cm in at least 100 grid cells within the computational domain (which represents 0.2% of the wetted cells). Based on the tidal component analysis of the model results, these components are O1, K1, N2, M2, S2, K2, 2N2, M4, MS4 and MN4 (Fig. 3).

As in previous studies (Pickering et al., 2012; Ward et al., 2012; Pelling et al., 2013; Pelling and Green, 2014), we first investigate how a uniform sea-level rise affects the tides. For this purpose, we consider the following SLR values: −0.25, 0, +0.25, +0.5, +0.75, +1, +1.5, +2, +3, +5 and +10 m. This includes a control run corresponding to the present situation (SLR=0 m), as well as idealised scenarios that correspond to sea levels that are plausible for more or less distant times in the past or future. The −0.25 m scenario may be considered as a lower bound for the preindustrial sea level (Church and White, 2011; Wöppelmann et al., 2014; Hay et al., 2015; Mitrovica et al., 2015). According to the IPCC 5th Assessment Report, a sea-level rise of +0.25 m is likely by 2046–2065, regardless of greenhouse gas emissions, and the likely range for the high emissions scenarios is +0.5 to +1 m by 2100 (Church et al., 2013a), which does not exclude larger amounts (Church et al., 2013b). For example, Jevrejeva et al. (2014) estimate that there is a probability of approximately 5% of exceeding +1.8 m by 2100. Importantly, sea level will continue to rise beyond 2100 (Church et al., 2013a) and is likely to reach several meters by 2200 (Kopp et al., 2014). Finally, consistent with Pickering et al. (2012), we also consider a +10 m SLR scenario. This scenario would have major geomorphologic impacts on coastal zones, greatly exceeding the range of uncertainties covered by the “flood”/”no flood” cases considered in this article. However, this scenario is possible over the next 3–4 centuries if all fossil fuel resources are consumed (Winkelmann et al., 2015; Clark et al., 2016).

3. Tides and sea-level rise

3.1. Tidal water levels

Fig. 4 illustrates the influence of SLR on the whole tidal curve based on several tide gauges used for model validation. Here, we focus on the mean spring tide. There are changes in high and low tide levels, as well as a temporal shift, and, depending on the location in question, changes in the shape of the curve.

In the following analysis, we focus on the effects of SLR on high tide levels (ξ_{max}). In each grid cell, we compute the difference (here called $\Delta\xi_{max}(SLR)$) between the maximum tidal water level reached over the

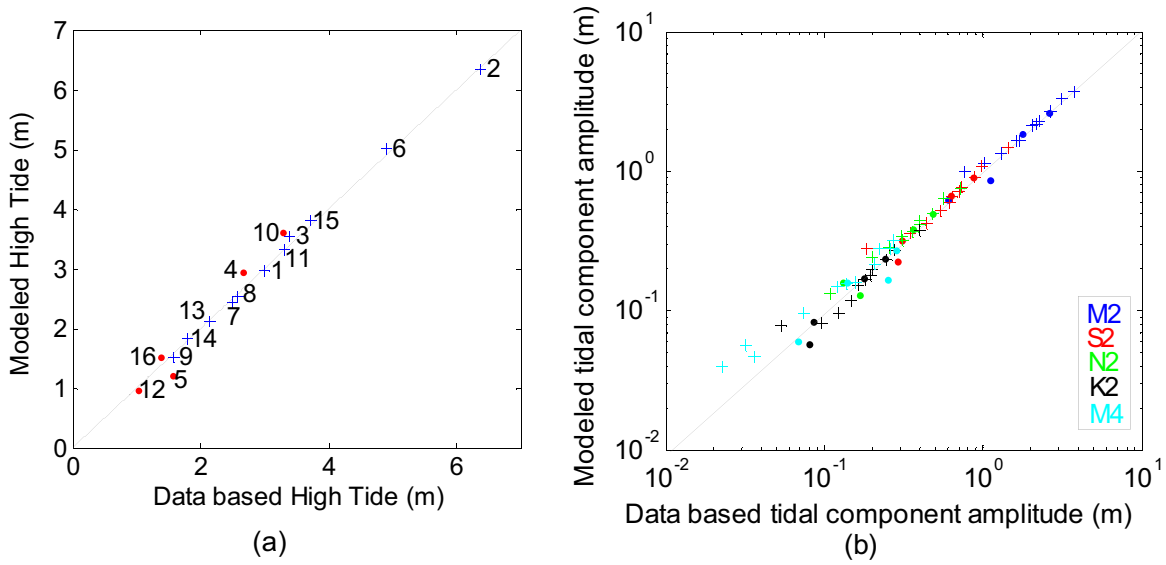

Fig. 2. (a) Modeled versus data-based highest annual tide (for the year 2009) for each site. The numbers refer to the tide gauge names (see Fig. 1a); (b) Modeled versus data-based tidal component amplitudes for 5 selected tidal components. + and • indicate sites with relative errors for the highest tide that are smaller or larger than 5%, respectively.

simulated year for a given SLR scenario (ξ_{max}(SLR)) and the maximum reached for the control case (ξ_{max}(SLR=0)). For the sake of readability, $\Delta\xi_{max}$(SLR) will be written as $\Delta\xi_{max}$. To compare the spatial patterns of tidal water level changes for several SLR scenarios, we focus on the ratio $\Delta\xi_{max}$/SLR. Fig. 5 shows the results for the +1, +2 and +5 m scenarios, with ξ_{max}(SLR=0) plotted in the left column. $\Delta\xi_{max}$/SLR ranges from −15% to +15% of SLR. The most negative values are observed in the western English Channel, and the most positive ones are observed in the southern North Sea, the eastern English Channel and the Irish Sea. For instance, the Bay of Mont Saint-Michel exhibits a decrease of 15 cm for an SLR of +1 m.

Fig. 5 also provides information on spatial similarity and proportionality of tidal changes (i.e., at a given location, does $\Delta\xi_{max}$/SLR always have the same sign and approximately the same value, regardless of the SLR scenario?). Over most of the domain, the effect of SLR appears to be spatially similar, and a proportional relation is observed between SLR and tidal changes. However, there are two main areas where the sign of tidal change depends on the magnitude of sea-level rise, and these areas occur in northeastern Scotland (Muray Firth, where $\Delta\xi_{max} > 0$ for SLR=+1 m, while $\Delta\xi_{max} < 0$ for SLR=+5 m) and along the western coast of Denmark ($\Delta\xi_{max} < 0$ for SLR=+1 and +2 m, while $\Delta\xi_{max} > 0$ for SLR=+5 m). In terms of proportionality, focusing on areas where changes have the same sign regardless of the SLR value, the $\Delta\xi_{max}$/SLR ratio appears to be almost constant in some areas (e.g., western English Channel), whereas it changes in other areas (e.g., in the Seine Bay or the central southern part of the North Sea).

To better assess the areas of spatial similarity and proportionality, we apply the following method within a given SLR range to each grid cell. First, the sign of the ratio $\Delta\xi_{max}$/SLR is computed in each grid cell and for each SLR value. If the sign changes with the SLR values, the cell is rejected. Otherwise, the sign (i.e., a binary value) is plotted (Fig. 6a). By mapping these binary values, the areas of spatial similarity can be identified. Then, changes are considered proportional to SLR in a given grid cell if the following 3 conditions are met: (1) they are spatially similar, (2) the correlation between $\Delta\xi_{max}$ and SLR is strong ($r > 0.9$) and significant (p-value < 0.05), and (3) the standard deviation of $\Delta\xi_{max}$/SLR is sufficiently small (here, less than 0.02). In this case, the coefficient of proportionality between SLR and tidal changes (which is called $a_{\xi_{max}}$ and is obtained by linear regression such that $\Delta\xi_{max}=a_{\xi_{max}}$ x SLR) is plotted (Fig. 6b). Maps of spatial similarity and proportionality coefficients have been drawn for three ranges of SLR values: G1 ([−0.25 to 1] m), G2 ([−0.25 to 2] m), G3 ([−0.25 to 10] m). Fig. 6a shows that the changes are spatially similar over most of the domain (70% of the domain for the G2 SLR range). The main patterns are as follows. Consistent negative patterns are located northwest of Scotland, in the western English Channel, in the Shetland Sea and north of the Southern Bight; positive patterns occur mainly in the North Sea, the Irish Sea, the eastern English Channel and along the French Atlantic coast. However, changes for the largest SLR range (G3) appear less spatially similar than for the smaller ranges (G1 and G2), especially in the Celtic Sea and around the M2 amphidromic points, probably due to SLR-induced migration of the amphidromic points (Fig. 7a). Whereas the amphidromic points (APs) of the Irish Sea, Celtic Sea and the English Channel are relatively stable, the Danish AP migrates to the northwest, and the 2 last North Sea APs migrate east-northeast (see, e.g., Pickering et al. (2012) for a discussion on AP migration). The central North Sea AP is the one that migrates furthest (> 10 km for SLR=2 m). Larger migration distances are obtained for larger SLR values. Over the entire area, the $a_{\xi_{max}}$ rates (Fig. 6b) indicate water level changes ranging from −15% to +15% of SLR (i.e., $-0.15 \leq a_{\xi_{max}} \leq +0.15$). The largest increase is observed in the German Bight, and the largest decrease is observed in the western English Channel. Again, whereas both the G1 and G2 SLR ranges produce very similar results, the largest SLR range (G3) leads to reductions in correlation and proportionality between the changes in maximum water levels and SLR. Thus, over most of the domain, $\Delta\xi_{max}$ is proportional to SLR when SLR ≤+2 m.

Fig. 8 (“no flood” case) shows the evolution of $\Delta\xi_{max}$ versus the SLR scenarios at three points (A, B, C, see Fig. 1a) located in areas of significant change: the western English Channel, the Irish Sea and the Wadden Sea. We should keep in mind the results provided by Fig. 6 for these locations: $\Delta\xi_{max}$ is similar (that is, the sign is unchanged) at the three points; $\Delta\xi_{max}$ is proportional to SLR for the ranges G1, G2 and G3 at points A and B; and $\Delta\xi_{max}$ is proportional to SLR only for ranges G1 and G2 at point C (there is no value for the Wadden Sea in Fig. 6b3). Fig. 8 illustrates this behavior and shows that the linear approximation of ξ_{max} changes with SLR up to SLR=+2 m is an imperfect but reasonable approximation for these locations. Based on the above results, we will mainly focus on changes induced by sea-level rises smaller than or equal to 2 m (i.e., range G2), and discuss the more extreme sea-level rise scenarios selectively.

The evolution of the minimum water level (ξ_{min}, figure not shown) exhibits, within the G2 range, an overall symmetry with the maximum water level changes: (1) $\Delta\xi_{min}$ is positive (negative) where $\Delta\xi_{max}$ is negative (positive), so that there is a decrease (increase) in the tidal

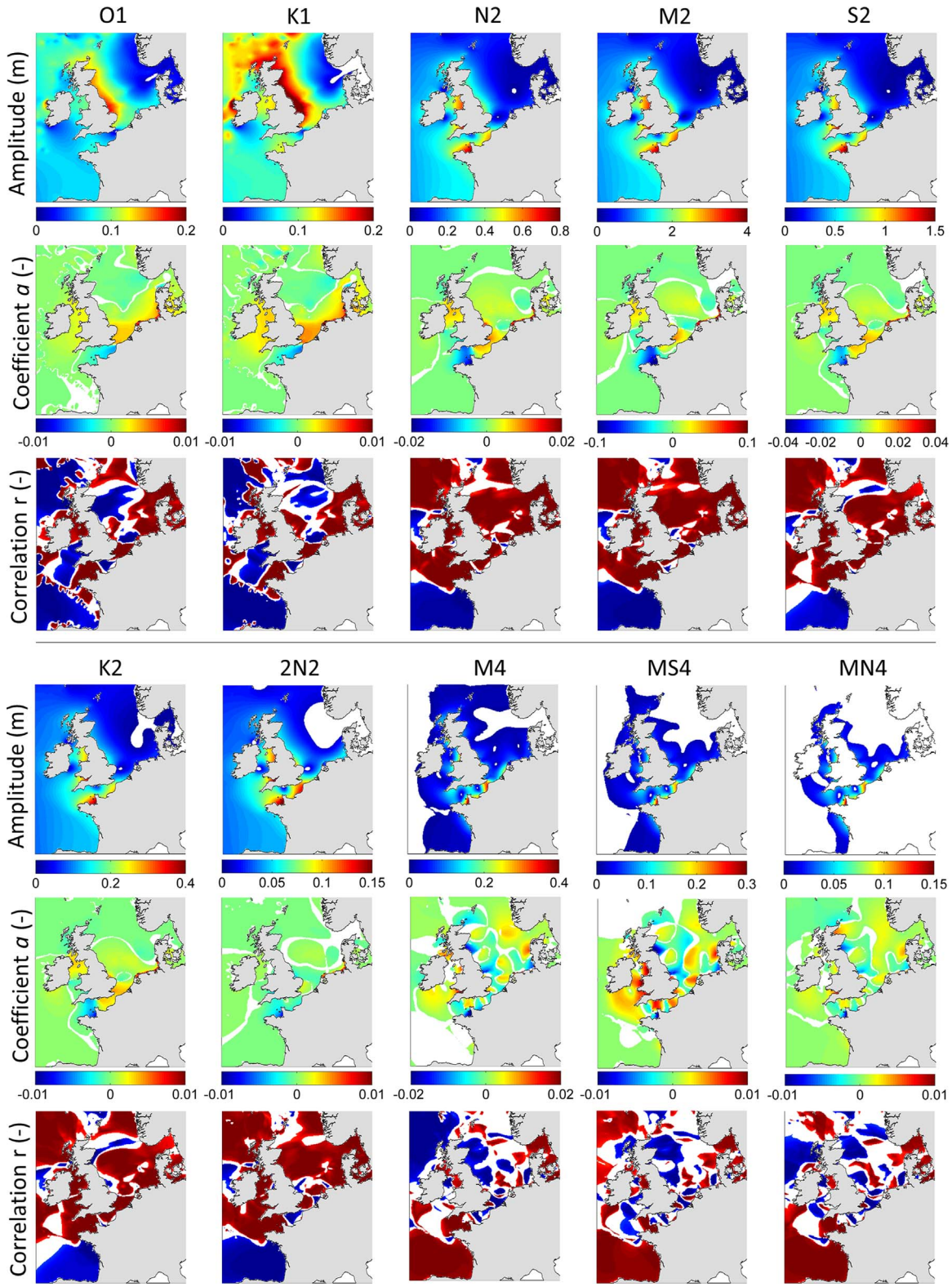

Fig. 3. Amplitudes of tidal components for the control scenario (SLR=0 m) (white: amplitudes smaller than 0.01); coefficients $a_{CST_{amp}}$, for areas of spatial similarity and proportionality (see the text for more explanation); maps of correlation coefficient r between $\Delta\xi_{max}$ and ΔCST_{amp} (red: r > 0; blue: r < 0; white: p-values ≥0.05).

range; (2) areas with large $|\Delta\xi_{min}|$ correspond to areas with large $|\Delta\xi_{max}|$. However, there are local exceptions to this symmetry, e.g., north of Ireland, north of the UK and along the French Atlantic coast. These areas correspond to sites with increasing tidal asymmetry (for an example, examine the tidal curve from La Rochelle shown in Fig. 4).

To conclude, the changes in maximum water level are almost proportional to SLR at most locations within the study area, as long as SLR does not exceed +2 m. The largest changes (positive or negative) are observed in the western English Channel, the Irish Sea and the German Bight (especially the Wadden Sea).

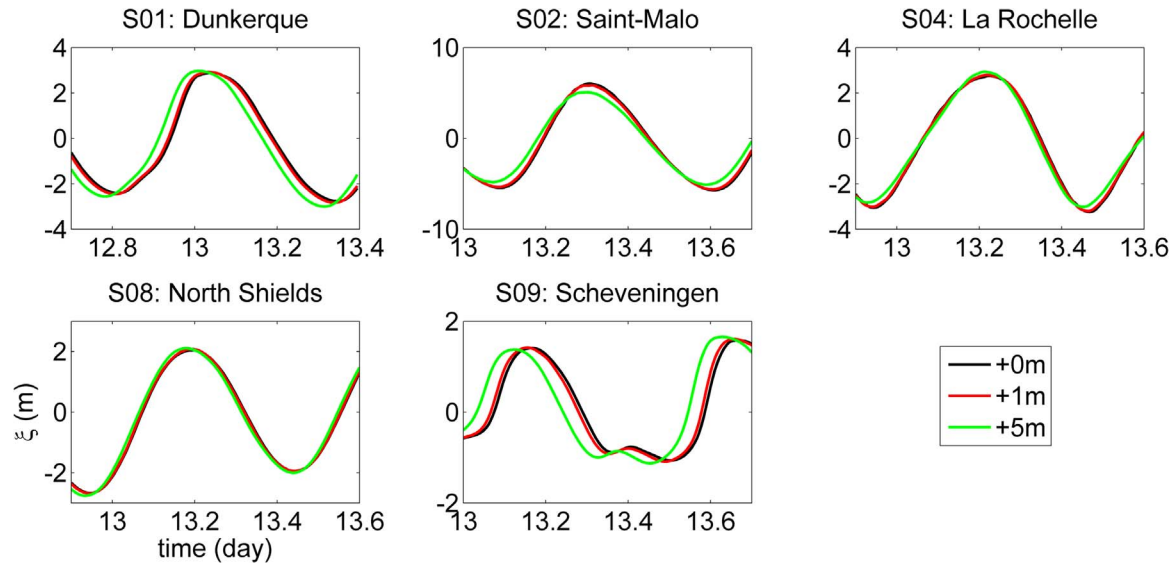

Fig. 4. Tidal curves from the S01, S02, S04, S07, S08, and S09 tide gauges (see Fig. 1a for locations) for a mean spring tide (equivalent to tidal forcing conditions occurring on 12–13 January 2009). These tide gauges are located in areas where tidal water level changes are proportional to SLR (see Section 3.1), in order to more easily illustrate the effects of SLR on the tides.

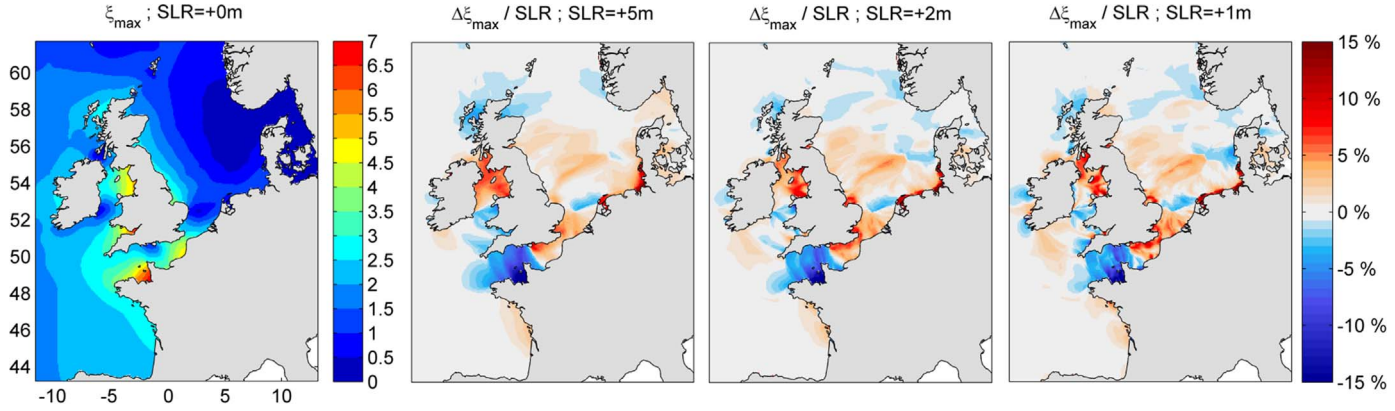

Fig. 5. Absolute values of maximum high tide level (ξ_{max}) for the control scenario (SLR=0 m) and relative changes in the maximum water level ($\Delta\xi_{max}$/SLR).

3.2. Tidal components

Fig. 3 shows the patterns of the main tidal components and their trends. For SLR=0 m, N2, M2, and S2 are the dominant tidal components, which have amplitudes of tens of centimeters over most of the domain. The other components reach tens of centimeters locally. Fig. 3 also shows the coefficient of proportionality ($a_{CST_{amp}}$) between SLR and the change in tidal component amplitude, as computed for the G2 SLR range. First, the changes in the amplitudes of the tidal components appear to be spatially similar and proportional to SLR over a large part of the domain. M2 exhibits the largest variations, and $a_{M2_{amp}}$ reaches −0.1 and +0.1, (i.e., −10% and +10% of the sea-level rise). In other words, its variations are similar to those of the maximum water level ($a_{\xi_{max}}$). There is also a strong similarity between the patterns of M2 change and maximum changes in water level. S2 and N2 exhibit similar patterns but with smaller coefficients; $a_{S2_{amp}}$ and $a_{N2_{amp}}$ range from about −0.03 to +0.03. The quarter-diurnal components M4 and MS4 have completely different patterns of change and exhibit smaller variations (relative to SLR), with $a_{CST_{amp}}$ values in the range [−0.01; +0.01]. However, in terms of changes relative to the tidal component amplitude (i.e., $a_{CST_{amp}}$ normalized by the tidal component amplitude when SLR=0, named $\hat{a}_{CST_{amp}}$), the quarter-diurnal components are those that show the largest changes. For example, changes in $\left|\hat{a}_{M4_{amp}}\right|$ can be larger than 100%, especially around the amphidromic points in the north-eastern part of the North Sea (figure not shown), whereas the maximum change in $\left|\hat{a}_{M2_{amp}}\right|$ is approximately 30%.

To relate the variations in the maximum tidal water level to those of the amplitudes of the tidal components, the correlation coefficients between $\Delta\xi_{max}$ and ΔCST_{amp} were computed in every grid cell. The correlations are significant (p-value ≥0.05) in most of the grid cells (Fig. 3). Areas without significant correlations (in white) are observed mainly around the amphidromic points, and their extents are larger for the quarter-diurnal components. Comparison of Fig. 6b2 and Fig. 3 ($a_{CST_{amp}}$ and the correlation coefficient r) shows that:

(1) North of the UK, in the Celtic Sea and in the western English Channel, a decrease in ξ_{max} would be related to a decrease in the semi-diurnal components.
(2) In the North Sea and in the Irish Sea, an increase in ξ_{max} would be related to an increase in the semi-diurnal components.
(3) Along the French Atlantic coast, an increase in ξ_{max} would be related to an increase in the quarter-diurnal components.

Thus, the semi-diurnal components determine the main patterns of change throughout the study area, with the exception of the French Atlantic coast, where the quarter-diurnal components play a significant role. The other components obviously contribute to these patterns, but

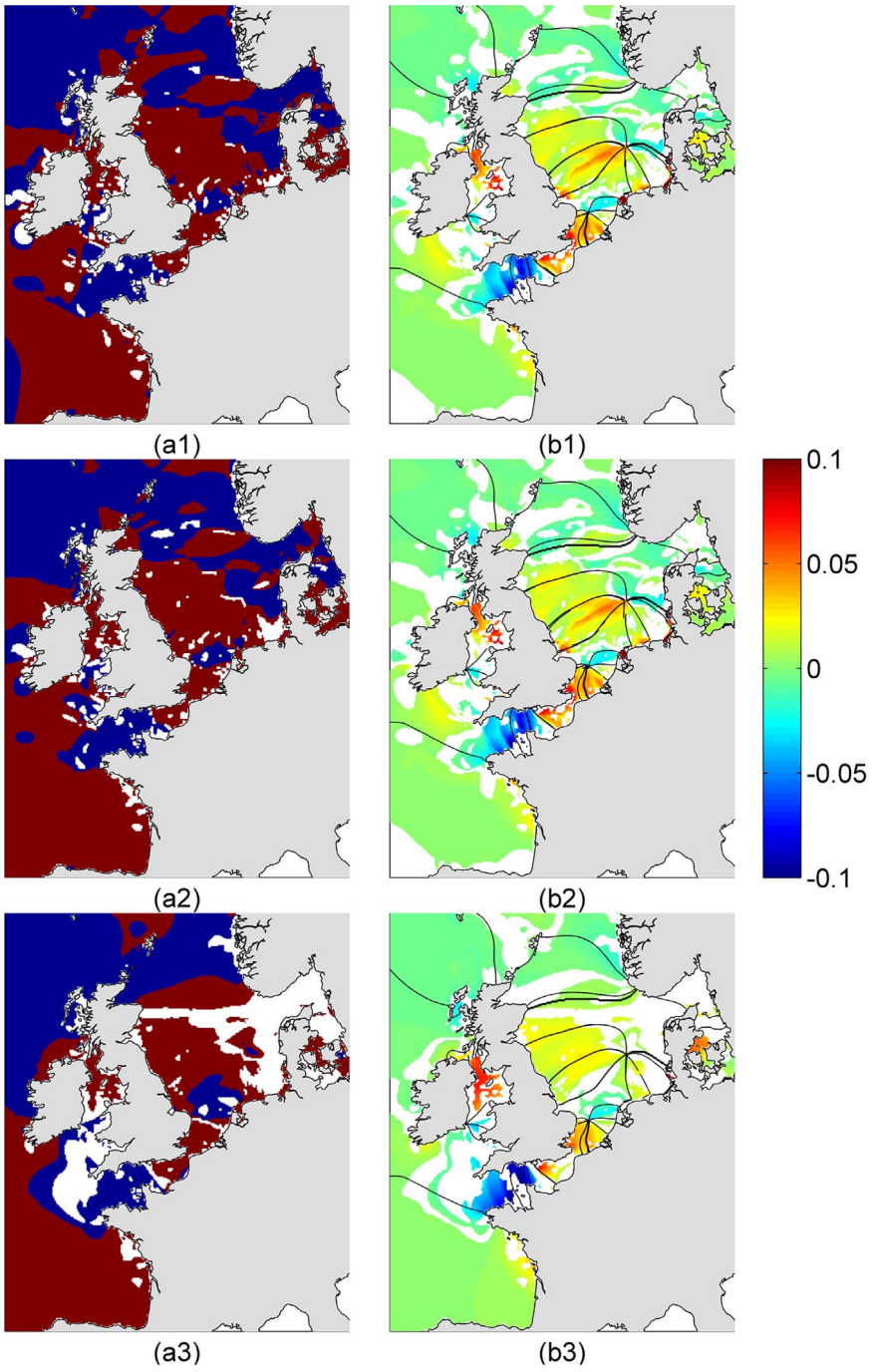

Fig. 6. Changes in ξ_{max} versus SLR ("no flood" option). (a) Areas of spatial similarity (blue: $(\Delta\xi_{max}/SLR) < 0$ regardless of the SLR value; red: $(\Delta\xi_{max}/SLR) > 0$ regardless of the SLR value; white: the sign of $(\Delta\xi_{max}/SLR)$ depends on the SLR value); (b) Maps of the values of the coefficient $a_{\xi_{max}}$ (white: areas where correlation, spatial similarity and proportionality criteria are not met – see text). 1, 2 and 3 indicate results for the following analyzed SLR ranges: [−0.25 – 1 m], [−0.25 – 2 m], [−0.25 – 10 m]. Lines indicate M2 phases (for SLR=0 and the "no flood" case) every 2 h, with the thick line indicating the 0 h phase.

mainly by modifying the intensity of the changes rather than the sign.

To complete the analysis, Fig. 7a shows M2 phase changes for SLR= +2 m: the dominant pattern represents a phase advance (i.e., an earlier arrival of the M2 wave). Along the Dutch and German coasts, the phase advance can reach 30 min (which is also visible in Fig. 4, for example at the Dutch site S09), whereas there is a phase delay of up to 20 min along the Norwegian coast. To a first approximation and at the scale of the European Shelf, assuming that the tide is a shallow water wave with a speed of $c = \sqrt{gD}$, the overall phase advance can be explained, as in Pickering et al. (2012), by an increase in speed as the water depth (D) increases. At a more local scale, the observed phase delays seem to be related to the migration of the amphidromic points.

4. Physical mechanisms and effects of different flooding options

Several mechanisms could explain the tidal changes induced by SLR. These mechanisms include reduced damping (due to increases in the water depth), changes in the resonant periods of the system (due, for instance, to changes in wave celerity induced by the greater water depth), and increased reflection at the coast (in the case of a "no flood" option). We investigate these mechanisms considering sea-level rises less than or equal to 2 m, and we provide a site-by-site analysis in Section 4.4.

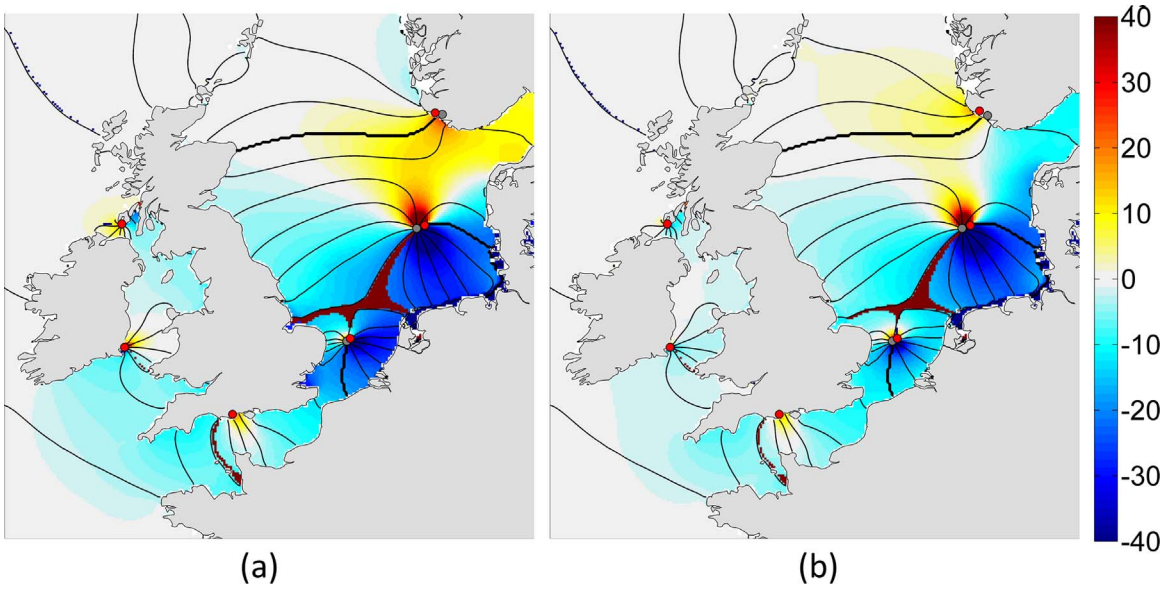

Fig. 7. M2 phase changes (in minutes) for SLR=2 m in comparison with the control scenario SLR=0 m, for the "no flood" (a) and "flood" (b) cases. Phases are plotted every hour. Thick lines indicate the 0 h phase, and the gray and red points indicate the amphidromic points for SLR=0 m and SLR=2 m, respectively.

4.1. Reduced damping

The effect of reduced damping is investigated through computations with an SLR value equal to 0; however, a bed friction drag coefficient Cd is used to account for sea-level rise, so that Cd/D remains constant regardless of sea-level rise. The bed friction follows a Strickler formulation in our hydrodynamic model. This condition is written in a Strickler form:

$$K(SLR) = K_0 \cdot \left(\frac{SLR}{D_0} - 1 \right)^{2/3} \quad (1)$$

with the subscript 0 indicating the K and D values for the control scenario SLR=0. This implies a non-uniform Strickler distribution. We consider a sea-level rise of 2 m. Fig. 9a shows the corresponding Strickler values K(SLR=2). The ξ_{max} changes induced by the reduced damping K(SLR=2) (Fig. 9b) and by a sea-level rise of 2 m (Fig. 9c) are of a similar order of magnitude (centimeters). Fig. 9d compares the sign of the ξ_{max} variations; the patterns appear to be consistent in many areas (especially in the eastern part of the English Channel, the southern part of the North Sea, and the Irish Sea). The main areas of discrepancy are in the western English Channel and parts of the Celtic Sea, where the reduced damping induces an increase in ξ_{max}, whereas an SLR of +2 m induces a decrease in ξ_{max}. In the Bay of Biscay, the pattern is reversed; the reduced damping and the sea-level rise induce a decrease and an increase in ξ_{max}, respectively. These results suggest that (1) a significant part of the tidal changes would be due to the reduced friction induced by the SLR, especially in the eastern English Channel, the southern part of the North Sea and the Irish Sea; (2) the reduced friction alone cannot explain the changes observed in the western English Channel, parts of the Celtic Sea and the Bay of Biscay.

4.2. Resonance

The amplitudes of tides on the Western European shelf is related to resonance phenomena. To check whether a sea-level rise would modify the resonance properties and whether the resonance period T_R would move closer to (or further from) the tidal component periods, we estimated the resonance period for the SLR scenarios of 0 and 2 m, using an approach similar to that of Liang et al. (2014) and Bertin et al. (2012). (1) A series of runs is performed, imposing sinusoidal waves with an amplitude of 0.1 m and a period varying from 3 h to 27 h at the open boundaries of the model, (2) computation of the amplification

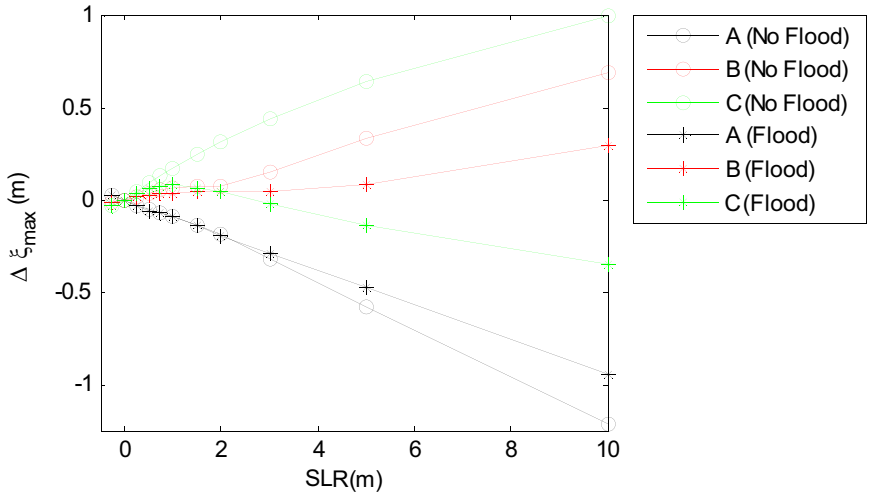

Fig. 8. $\Delta\xi_{max}$ versus SLR for points A, B and C (see locations in Fig. 1a) for the "no flood" and "flood" scenarios.

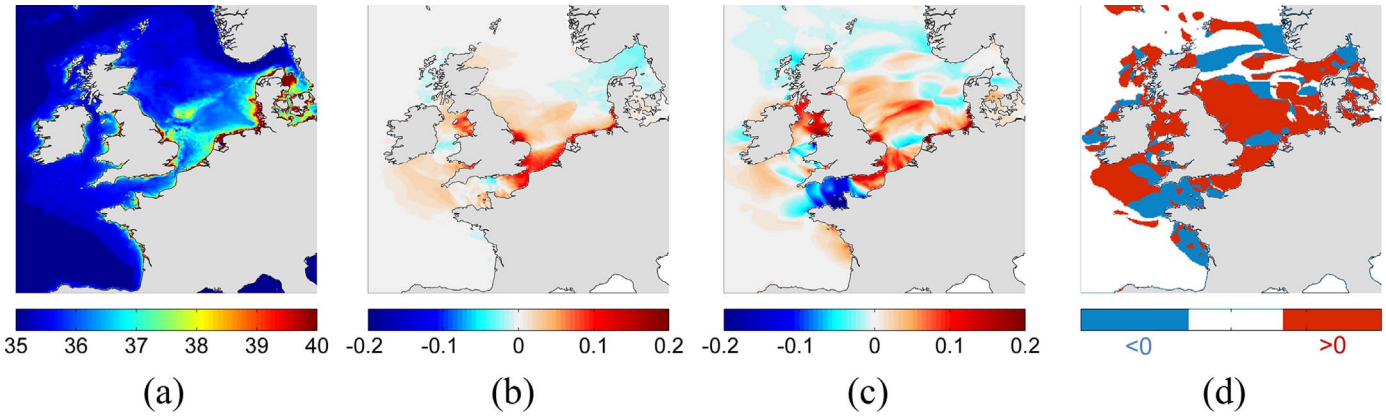

Fig. 9. (a) Strickler coefficient K(SLR=2) ($m^{1/3}$ s^{-1}); (b) changes in high tide level (m) for SLR=0 and K(SLR=2), i.e., $\Delta1=\xi_{max}$(SLR=0, K(SLR=2))−ξ_{max}(SLR=0, K_0); (c) changes in high tide level (m) for SLR=2 m and K"K_0, i.e., $\Delta2=\xi_{max}$(SLR=2, K_0)−ξ_{max}(SLR=0, K_0); (d) sign(Δ1)/sign(Δ2) (white: Δ1 and Δ2 smaller than 0.01 m).

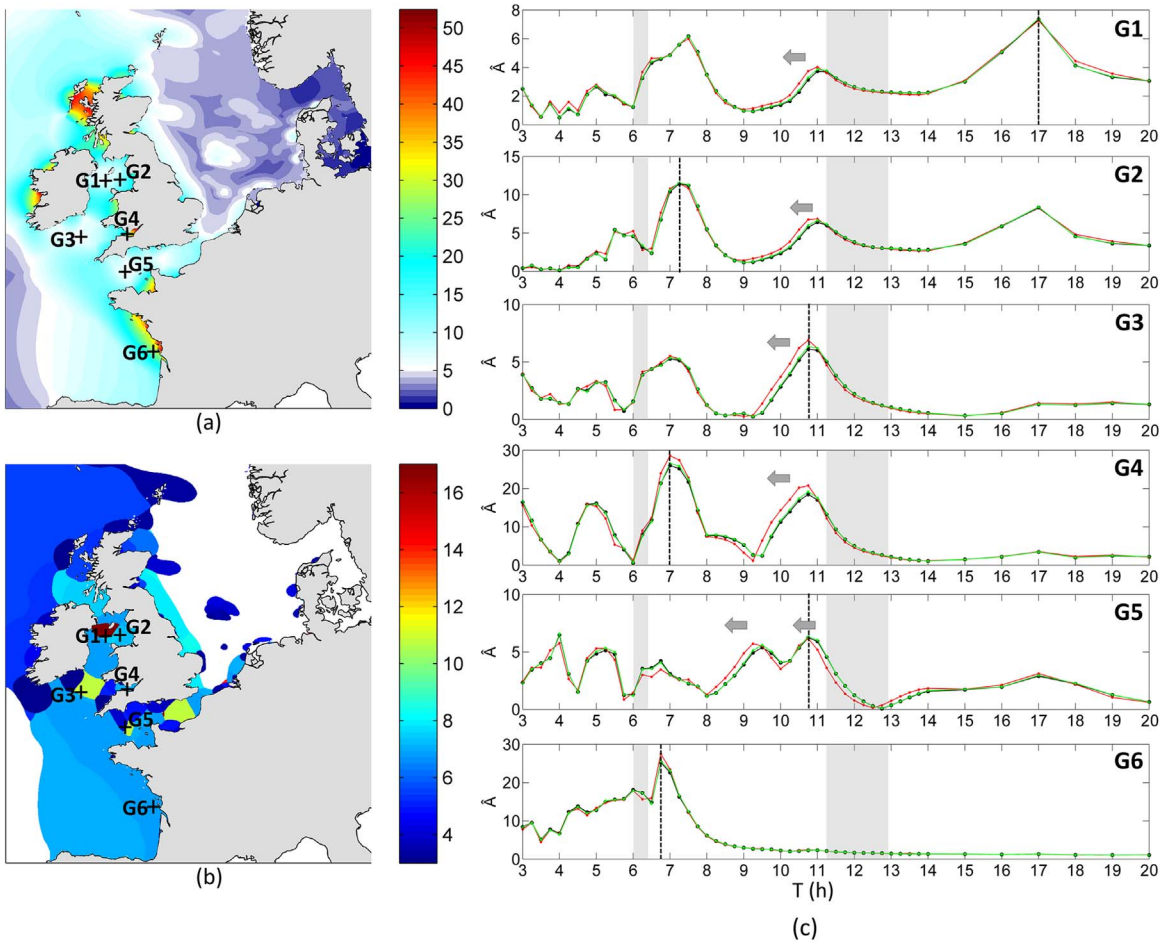

Fig. 10. (a) Amplification factor Â (-); (b) period (h) corresponding to the maximum of Â; (c) amplification factor Â (-) as a function of the period of imposed offshore boundary conditions for SLR=0 and K_0 (black), SLR=2 m and K(SLR=2) (red), and SLR=0 and K(SLR=2) (green). Gray areas indicate the bands of the (semi and quarter-diurnal) tidal component periods. The locations of the 6 points are indicated in (a) and (b). The results were obtained with the "no flood" option.

ratio Â, defined as the ratio between the local wave amplitude and the amplitude at the open boundary of the computational domain (i.e., 0.1 m).

Fig. 10a shows the maximal amplification ratio Â. It highlights areas of strong amplification (Â > 30), such as the central part of the French Atlantic coast, the Bay of Mont Saint Michel and the Bristol Channel. Fig. 10b shows the corresponding periods and highlights areas with periods of 5 h, 7–8 h, and 11 h, as well as the northwestern Irish Sea, which displays a period of 17 h. In the following discussion, we focus on areas where the changes induced by sea-level rise are in the opposite direction to those induced by reduced damping (Fig. 9d), i.e., the Celtic Sea, the Bristol Channel, the western English Channel and the central part of the French Atlantic coast. The Irish Sea, where SLR-induced water level changes are related to resonance property changes (Pelling et al., 2013a), is also investigated. Fig. 10c provides, for these areas, the amplification factor Â as a function of the period of the signal imposed at the offshore boundaries. Although we do not aim to achieve a detailed or precise analysis of the resonance phenomena, we validate the above pragmatic approach by comparing the resonance period obtained for the SLR=0 scenario ("no flood") with resonance periods

from the literature. Most of the reported resonance periods are based on theory and provide values for idealised cases, so that their application to real sites may not be exact but should provide a good enough approximation for validation purposes. For instance, for a semi-enclosed basin, the (quarter-wavelength) resonance period T_R can be approximated by $T_R = 4L/\sqrt{gD}$, with L being the basin length. The estimate of the resonance period in the Celtic Sea and Bristol Channel made by Pugh (1987) is based on this approach.

For points G1 to G5, local maxima are observed at T_R~5 h, T_R~7 h and T_R~11 h. In the north-western Irish Sea (G1), the most amplified perturbation occurs at T_R=17 h, which agrees qualitatively with the value of 15.7 h obtained using the quarter-wavelength resonance formula (Pelling et al., 2013a). Farther east (G2), this mode is still present with the same amplification factor, but the most amplified perturbation is observed for T_R=7.25 h. In the Celtic Sea (G3), the most amplified perturbation occurs at T_R=10.75 h. Pugh (1987) estimated that the resonance period should be slightly larger than 12 h, but smaller than the semi-diurnal tidal component periods, using the quarter-wavelength resonance formula. Both estimates give a resonance period smaller than the M2 period. In the Bristol Channel (G4), several modes are observed (e.g., 5 h, 7 h, 10.75 h), but the dominant one, as for G2, is T_R=7 h. This is in agreement with the study of Liang et al. (2014). In the western English Channel (G5), there are also several modes, and the most amplified one occurs at T_R=10.75 h. Finally, along the central part of the French Atlantic coast, there is a broad band of amplified modes between T~4 h and T~7.5 h with a maximum at T_R=6.75 h. Such a broad band was also observed by Bertin et al. (2012), but the maximum amplification occurred at a smaller period (T_R~5.3–5.8 h). For each of the above locations, the local maximum of Â does not fall within the quarter-diurnal or semi-diurnal band of the tidal components (gray area in Fig. 10c). However, the quarter- and semi-diurnal tidal component periods fall in a regime with significant amplification (e.g., Â~18 at point G6 for the quarter-diurnal tidal periods), confirming that resonance phenomena play a role in the local amplitudes of quarter- and semi-diurnal tidal components.

Fig. 10c shows that the main change induced by sea-level rise (here, +2 m) is a shift in the semi-diurnal resonance period (T_R~11 h) toward smaller periods (Fig. 10c), i.e., further from the band of the semi-diurnal tidal components. In contrast to the Irish Sea, the Celtic Sea and the Bristol Channel, the changes in the resonance periods along the central part of the French Atlantic coast (G6) are very small. Fig. 10c also shows that a reduced damping scenario (K(SLR=2) and SLR=0) induces only a few changes in the resonance periods and amplitude, suggesting that the changes in resonance properties are mainly induced by changes in tidal wave characteristics, rather than by reduced damping.

4.3. Effect of the flooding option: flood versus no flood

Additional simulations are done with the "flood" option in order to (1) assess the effects of the flooding option on the results obtained in Section 3 and thus the reliability of the conclusions, (2) provide material for the analysis of mechanisms.

First, the M2 phase changes appear sensitive to the "flood"/"no flood" mainly in the North Sea, with a smaller tidal advance occurring in the southeastern part (along the coasts of Belgium and the western Netherlands) and a shift from phase advance to phase delay along the northern Danish and southern Norwegian coasts (Fig. 7b).

Second, the relative changes ($\Delta\xi_{max}$/SLR) obtained for both the "flood" and "no flood" scenarios have the same sign in most areas (57% of the domain) (Figs. 6a2 and 11a1). In some areas that previously showed an increase in ξ_{max}, a decrease is now observed (e.g., the German Bight, the Dutch coast and, to a smaller extent, the Irish Sea). In these areas, future tides will thus be mostly sensitive to coastal defense scenarios. The proportionality coefficients $a_{\xi_{max}}$ display the same order of magnitude in both scenarios (Figs. 6b2 and 11a2), while the areas with proportional behavior (colored areas in Fig. 11a2) are less widespread in the "flood" case, meaning that, compared with the "no flood" case, tidal changes are less proportional to SLR when the "flood" option is activated. Fig. 8 illustrates the influence of the "flood" option for a wide range of SLR values. (1) For the three locations A, B and C, the magnitudes of the changes decrease overall. (2) Contrary to the "no flood" case, changes at point C (Wadden Sea) do not display any proportionality with SLR ($\Delta\xi_{max}$ first increases to SLR=+2 m and then decreases to negative values for SLR larger than +3 m).

To provide estimates of probable trends in the future, we compute the mean of the $a_{\xi_{max}}$ coefficients obtained for the "flood" and "no flood" scenarios (Fig. 11a2, b2). The areas consistently characterized by the largest changes are the western English Channel ($a_{\xi_{max}} \sim -0.15$) and the northern channel of the Irish Sea ($a_{\xi_{max}} \sim +0.06$) (Fig. 13b2). In addition, $a_{\xi_{max}} \sim +0.02$ in the central part of the North Sea. At a finer spatial scale, for SLR at least up to +2 m, small but consistent increases are observed in front of several estuaries, such as the Gironde (France, Atlantic coast) and the Tyne (England, North-East). In these areas, this consistency suggests that the estimated trends are realistic.

Resonance characteristics have also been computed for the "flood" case (figure not shown). Overall, for SLR=0, the maximum values of the amplification ratio Â are slightly smaller than in the "no flood" case, whereas the patterns of the periods of the most amplified mode are very similar. A sea-level rise of 2 m induces changes in the amplitudes, but not in the periods.

4.4. Site-by-site analysis in the "no flood" case

In the Irish Sea, for SLR=2 m, (1) there is no significant change in the resonance properties of the most amplified mode (T_R~17 h; Fig. 10c), (2) damping reduction produces patterns very similar to those obtained using a sea-level rise of 2 m (Fig. 9), (3) activating the "flood" option (i.e., reducing the reflection at the coast and increasing damping inland) leads to a smaller increase in ξ_{max} (e.g., Point B in Fig. 8). Thus, the two main processes causing the increase in ξ_{max} with SLR would be the reduced damping (via the friction term) and the increase in reflection at the coast. This interpretation differs from that of Pelling et al. (2013a), who suggested that changes are mainly linked to a shorter resonance period.

In the Celtic Sea, ξ_{max} increases in the western part and decreases towards the English Channel and north of Cornwall (Fig. 9c). Our modelling tests show that (1) a reduced damping leads to an increase in ξ_{max} (Fig. 9b); (2) over most of this area, similar changes are obtained in the "flood" case; (3) there is almost no change in resonance properties in the "flood" case, whereas there is a shift away from the tidal semi-diurnal component in the "no flood" case (see point G3 in Fig. 10c). Thus, tidal changes would result from reduced damping, counteracted by changes in resonance properties. This explains why ξ_{max} increases in some parts of the Celtic Sea and decreases in others.

Fig. 12 shows the changes for SLR=0.5, 1 and 2 m in the Bristol Channel. For the "no flood" case, the patterns do not change significantly from one SLR value to another. In the eastern and western parts, ξ_{max} increases and decreases, respectively. In the "flood" case, the results differ mainly in the eastern part, with ξ_{max} decreasing for SLR=0.5 m and slightly increasing locally for SLR=1 and 2 m. This suggests that reflection at the coast plays a significant role in the eastern part. In addition, reduced damping results in an increased maximum water level (Fig. 9b), whereas sea-level rise causes a shift of the 10.75-h resonance mode away from the periods of the semi-diurnal tidal components (Fig. 10 – point G4). Thus, ξ_{max} would result from the competition between reduced damping (and reflection) and changes in the resonance properties.

In the English Channel, ξ_{max} increases in the western part and decreases in the eastern part. A reduced damping (K(SLR=2)) leads to an increase in ξ_{max} for most of the English Channel (Fig. 9b), whereas

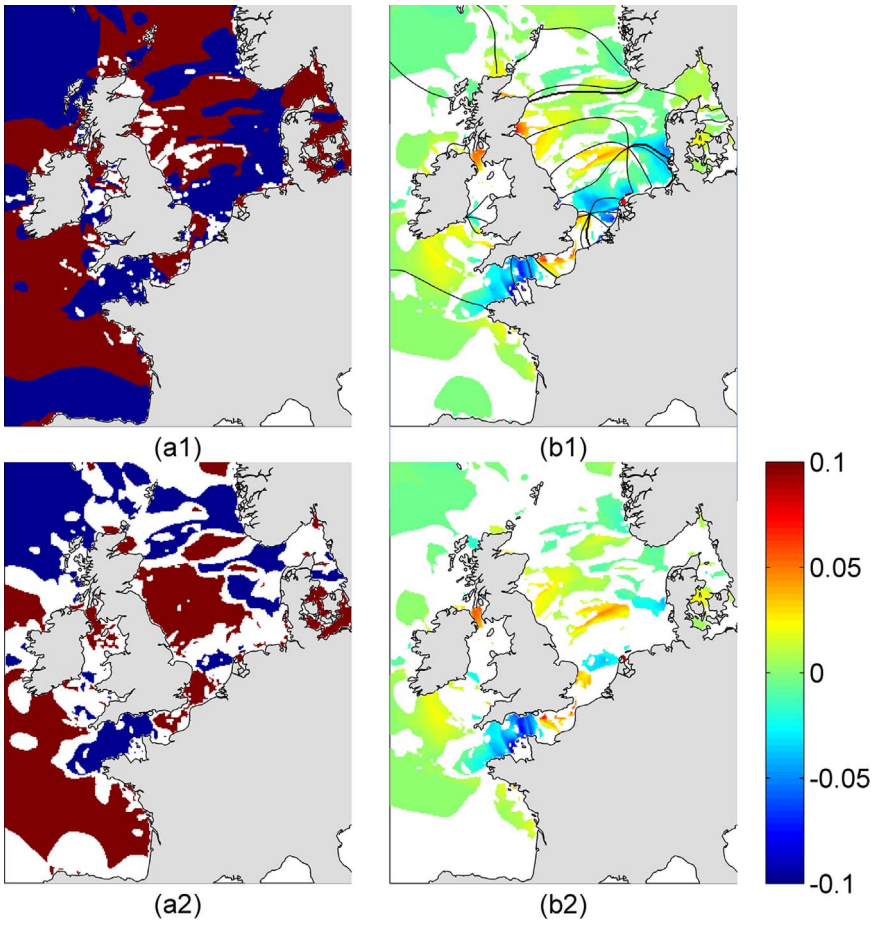

Fig. 11. (a) Areas of spatial similarity (blue: ($\Delta\xi_{max}$/SLR) < 0 regardless of the SLR value; red: ($\Delta\xi_{max}$/SLR) > 0 regardless of the SLR value; white: the sign of ($\Delta\xi_{max}$/SLR) depends on the SLR value); (b) values of $a_{\xi_{max}}$ for cases (1) where flooding is allowed, (2) taking into account both "flood" and "no flood" runs by computing the mean of $a_{\xi_{max}}$ values obtained for the "no flood" and "flood" cases, rejecting every grid cell where the sign of $a_{\xi_{max}}$ changes between the two cases. The computations are done for the G2 SLR range [−0.25–2 m]. Lines in (b1) indicate M2 phases (for SLR=0, "flood" case) every 2 h, with the thick line indicating the 0 h phase.

the shift in the two largest resonance modes (9.5 and 10.75 h) away from the periods of the semi-diurnal tidal components results in a decrease of ξ_{max}. Similar changes are obtained when flooding is allowed, suggesting that additional reflection at the coast does not play a significant role. Thus, the ξ_{max} decrease (increase) in the western (eastern) part would be mainly driven by changes in resonance

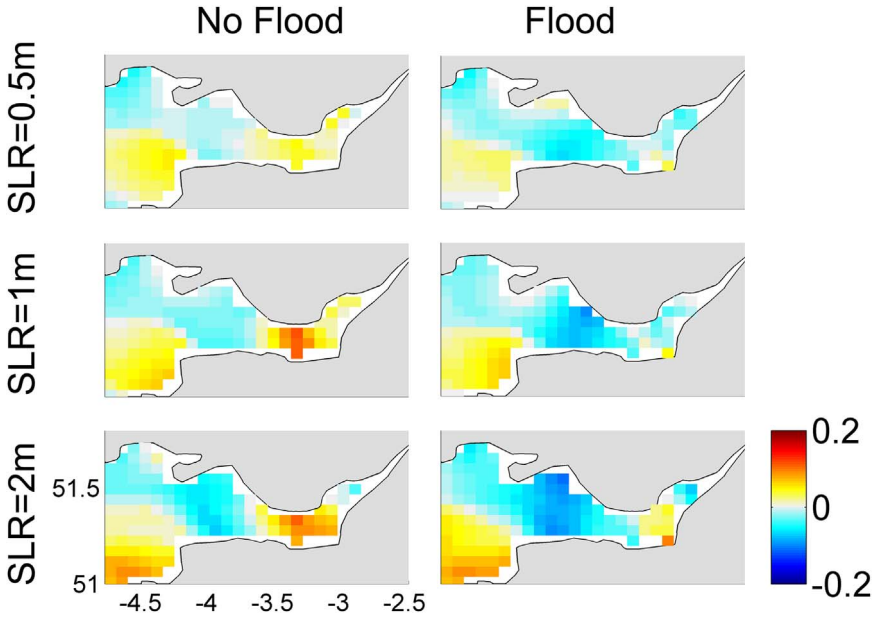

Fig. 12. Change (in meters) of the maximum tidal water level ξ_{max} in the Bristol Channel for three SLR values and the two "flood" and "no flood" options.

properties (reduced damping).

Along the German Bight coastline, both ξ_{max} and the M2 amplitude increase with SLR (in the G2 range). Based on Pelling and Green (2014), the SLR-induced tidal changes could be related to the increased energy flux entering the North Sea through the Dover Strait, so that the North Sea behaves less like a semi-enclosed basin. Indeed, there is a significant modification in the tide around the Dover Strait (Fig. 6b). In the "flood" case, both ξ_{max} and the M2 amplitude are decreasing in the German Bight, whereas the M2 amplitude along the eastern coast of the UK is almost the same with and without flooding (except in the Norfolk area). In addition, reduced friction (K(SLR=2)) produces an increase in ξ_{max} over a large part of North Sea, including the German Bight (Fig. 9b). Therefore, the increase in ξ_{max} ("no flood" case) in the German Bight would be related to reduced damping (smaller local dissipation) and increased reflection at the coast.

Along the central part of the French Atlantic coast, there is no change in the resonance period (G6, Fig. 10c), while reduced friction and sea-level rise produce decreases and increases in ξ_{max}, respectively (Fig. 9b,c). ξ_{min} also increases with SLR, so that the changes are not symmetric. Changes in the amplitudes of the M2 and M4 components have the same order of magnitude, but a decrease is observed for M2 and an increase for M4 (Fig. 13a1 and b1). M2 displays almost no phase changes, whereas M4 displays a significant negative change (−10° to −20°) (Fig. 13a2 and b2). The M4 phase relative to the M2 phase (2φM2−φM4) ranges from approximately 220° to 280°, corresponding to an ebb-dominant tide, for SLR=0 and from approximately 230° to 290° for SLR=2 m. This increased tidal asymmetry seems not to be related to the reduced friction (computation with the equivalent friction K(SLR=2) shows almost no change in the amplitudes and phases of M2 and M4) or to the decrease in the M2 amplitude (see the terms producing asymmetry in the 1D shallow-water equations in Parker (2007)). Because the "flood" case does not show any increase in asymmetry, it may be that the increased tidal asymmetry (and the increase in ξ_{max}) in the "no flood" case is likely due to increased reflection at the coast.

5. Discussion

5.1. Regional variability of sea-level rise

The above mechanisms analysis shows that SLR-induced tidal changes result from local and non-local processes. This is consistent with the simultaneous existence of areas that respond proportionally to SLR and others that do not (Section 3). These results are based on the assumption that sea level will rise uniformly. However, future sea-level rise will display regional variability (Church et al., 2013a). We therefore analyze to what extent tidal changes (relative to the local SLR) induced by a uniform or a non-uniform SLR would be significantly different by considering a synthetic idealised non-uniform SLR field, based on Slangen et al. (2014) (Fig. 14a). This SLR scenario corresponds to the current state of knowledge of the regional variability of future sea-level rise on the European continental shelf, given a global mean sea-level rise of 0.5 m by 2100 and the RCP4.5 climate change scenario.

Fig. 14b,c shows the relative water level changes obtained. To quantitatively assess the effect of non-uniform SLR, we compute, in each grid cell, the relative difference (Δ1−Δ2)/Δ2, with Δ1=(Δξ_{max}/

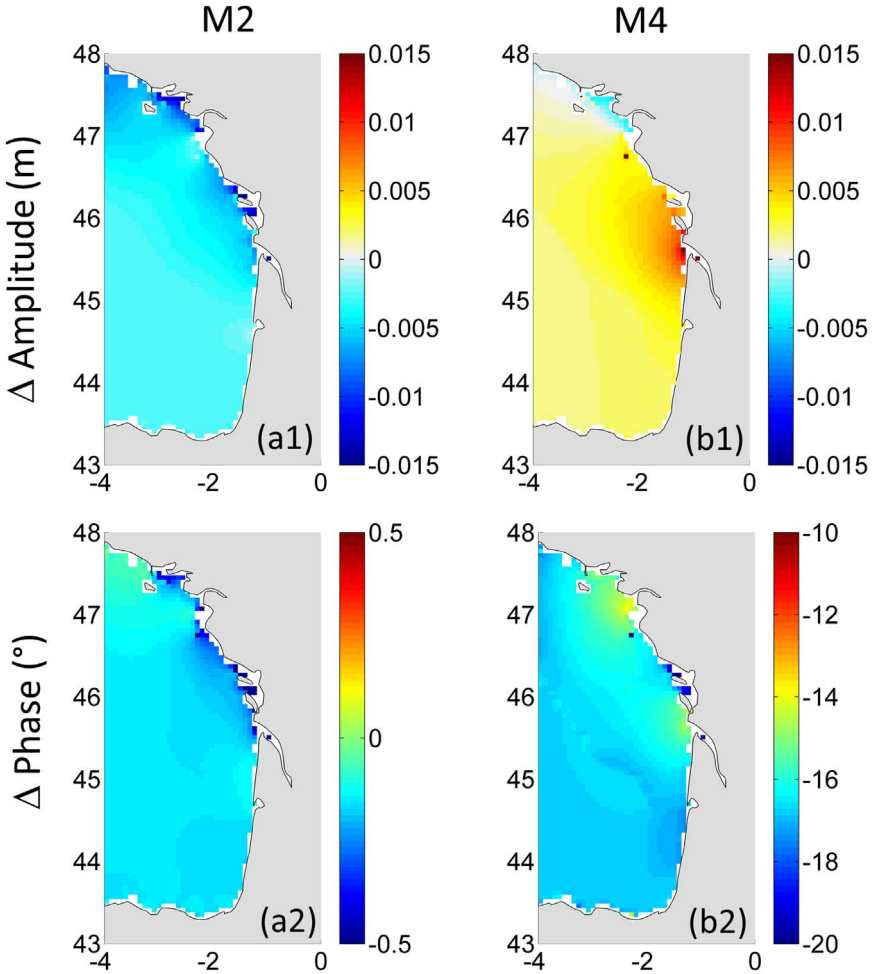

Fig. 13. Changes in tidal amplitude (1) and phase (2) for SLR=2 m, relative to SLR=0, for the M2 (a) and M4 (b) tidal components.

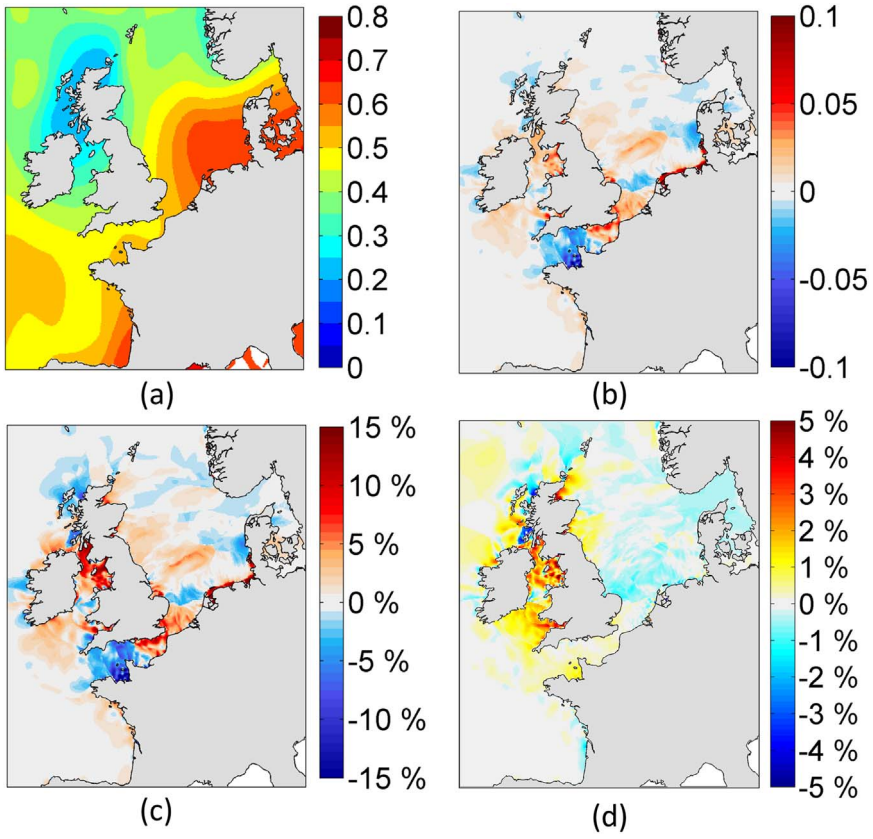

Fig. 14. (a) Non-uniform SLR (in meters); (b) absolute change $\Delta\xi_{smax}$ (in meters) for non-uniform SLR; (c) relative change $\Delta1=(\Delta\xi_{smax}/SLR)$ (in %) for non-uniform SLR; (d) relative difference $(\Delta1-\Delta2)/\Delta2$ (in %) with $\Delta2=(\Delta\xi_{smax}/SLR)$ for SLR=0.5 m.

SLR) for the non-uniform scenario and $\Delta2=(\Delta\xi_{smax}/SLR)$ for the SLR=0.5 m scenario (which is the scenario whose SLR value is the closest to the spatial average of the SLR values of the non-uniform scenario). Over most of the domain (92%), the differences are smaller than 1% (Fig. 14d), while most of the areas characterized by a response proportional to the uniform SLR (Section 3) display differences smaller than 1%. The largest differences can reach 10% and are observed mainly in the Irish Sea, the Celtic Sea, and the Bristol Channel and some bays, such as the Bay of Inverness. These differences are consistent with the mechanisms analysis (Section 4); the SLR-induced reduction in bed friction (a local process) could explain the overall similarity in terms of the orders of magnitude and signs between the non-uniform and uniform SLR-induced changes, whereas the increased reflection at the coast and changes in resonance properties (non-local processes) could explain the quantitative differences between the relative tidal changes induced by non-uniform and uniform SLR scenarios. Similar results are obtained from comparisons with the uniform SLR=1 m scenario. As the relative changes $(\Delta\xi_{smax}/SLR)$ obtained up to SLR=+1 m do not appear to be sensitive to the assumption of SLR uniformity in areas with tidal changes proportional to SLR, this prediction could be updated by combining maps of $a_{\xi_{max}}$ (Fig. 6b1) and other non-uniform future SLR predictions, insofar as the local SLR is smaller than or equal to +1 m. Given that the $a_{\xi_{max}}$ map obtained for the G2 range is similar to that obtained for the G1 range, we expect this conclusion to be valid for SLR values ≤2 m.

This test, which is based on existing knowledge of future SLR regional variability, provides a first quantitative prediction of tidal changes (high tide level) by 2081–2100 for the RCP4.5 scenario (Fig. 14b). It also highlights that taking into account SLR non-uniformity is useful in reducing uncertainties in future tidal changes, especially in areas displaying a non-proportional response to SLR.

5.2. Modelling assumptions

This study is based on assumptions which are essentially the same as those used in previous modelling studies. First, we assumed that the tidal components at the open boundaries of the computational domain (Fig. 1) are not significantly modified by sea-level rise. Pickering et al. (2012) justified this assumption using the following two facts: (1) the open boundaries are located in deep water and far from the shelf (thus, they are not influenced by tidal changes inside the domain), (2) the M2 changes in the open boundary areas are small (< 5 cm for SLR=+2 m). This is confirmed by Green (2010), who obtained small changes (~2.5 cm) in the M2 components along the open boundaries of our model for a 5 m SLR.

Furthermore, we have not considered the effect of morphological changes, such as changes in coastlines due to erosion/accretion or modification of the bathymetry and bedforms. However, such changes are theoretically affected by the SLR, as well as many other phenomena, such as waves, changes in the sediment budget or the effects of coastal defenses (e.g., Stive et al., 2002; Le Cozannet et al., 2014). Therefore, our capacity to anticipate future tide-SLR interactions is limited by our currently insufficient capabilities for producing long-term scenarios of shoreline and coastal morphology changes. A key factor is the morphological time scale of adjustment. For instance, the North Sea is characterized by many tidal sandbanks, which have doubling times of construction of a few hundred years, implying a total formation time of at least several thousand years (Idier et al., 2009). This timescale is much longer than the centennial timescale of expected sea-level rise. For other morphologies such as more dynamic bedforms (e.g., dunes) or shorelines, we can expect the morphological timescale to be closer to the scale of sea-level rise (e.g., Ranasinghe et al., 2012).

5.3. Comparison with previous studies

The results we obtained for the SLR=−0.25 m scenario (figure not shown) can be compared with observation-based studies (i.e., tide gauge analysis). First, Woodworth (2010) investigated recent changes in the main tidal components (M2, S2, K1, O1). With the exception of two locations (in the north of England and near Brest), our results show the same trend of recent increases in the M2 and S2 amplitudes along the Dutch and Danish coasts, as well as in the German Bight and the Irish Sea, and decreases along the east coast of England, in the Bay of Mont Saint-Michel and the Celtic Sea. Second, Mawdsley et al. (2015) investigated secular changes in tidal water levels. Our results show similar results on the European shelf. (1) There are areas with regionally consistent patterns of changes (e.g., the German Bight); (2) there are significantly more positive trends for high water levels and more negative trends for low water levels; and (3) the changes in high water level are spatially variable (in value and sign). Mawdsley et al. (2015) found no correlation between SLR and high water level changes. This is consistent with our study, which shows that, for the same SLR, changes can be very different from one site to another (e.g., Fig. 5), and, to a lesser extent, that some locations do not exhibit changes proportional to SLR (e.g., Fig. 6b1). In addition, we found changes in ($\Delta\xi_{max}$ / SLR) ranging from about −15% to +15%. Assuming that tide level changes are proportional to SLR and a rate of SLR of 3 mm/y (1992–2013) after Church et al. (2013a, 2013b) (SLR on the north-western European shelf is close to the global trend), such range would correspond to trends (in tidal range) ranging from about −0.9 to +0.9 mm/y. These values are of the same order of magnitude as the trends obtained by Mawdsley et al. (2015) on the Northern European shelf. Thus, a significant part of the tidal changes observed at tide gauges would relate to the effects of SLR.

Many modelling studies have investigated the effect of SLR on tides (see the review of Pickering et al. (2012)). We focus on the most recent studies (Pickering et al., 2012; Ward et al., 2012; Pelling et al., 2013; Pelling and Green, 2014). The related methods are summarized in Table 1. None of these studies provide maps of maximum water levels, but they all provide maps of M2 amplitude changes. Therefore, the comparison is limited to M2 changes. First, we focus on the results obtained by Pickering et al. (2012) and Pelling et al. (2013) for +2 m and +5 m SLR scenarios, under the "no flood" assumption. Our study provides patterns of M2 amplitude changes (SLR=+2 m) that are consistent with both studies. The only discrepancy is the positive trend along the Danish coast given in Pickering et al. (2012). In terms of magnitude, the three studies show changes of up to 10–15% of SLR. In terms of proportionality, Pickering et al. (2012) observe that changes in M2 amplitudes are not proportional to SLR, whereas the results of Pelling et al. (2013) and the present study show that, in the "no flood" case, these changes are proportional to SLR over most of the domain. Finally, we can refer to the study of Roos et al. (2011), in which sensitivity tests of SLR (0–2 m) conducted in the North Sea show that the patterns of increase and decrease in the M2 amplitude remain unchanged regardless of the SLR value. As in our study, strong increases in M2 were noted in the Dover Strait and the German Bight.

Ward et al. (2012) and Pelling et al. (2013) also considered the "flood" case, and investigated large SLR scenarios (≥2 m). Both studies noted a decrease in M2 amplitude for SLR=+2 m, and an increase for SLR=+5 m, in the Irish Sea. We obtained the same result (figure not shown). However, this does not mean that the high tide water level ξ_{max} will follow the same behavior. Indeed, our study suggests that ξ_{max} would increase for most parts of the Irish Sea, even when flooding is allowed. This highlights the importance of accounting for other tidal components when attempting to draw conclusions about tidal water levels. Next, we consider possible outcomes for smaller SLR values. Pelling and Green (2014) suggested that, in the Irish Sea, the M2 amplitude increases for SLR=+0.5 m and SLR=+1 m. This would mean that M2 amplitude first increases when SLR=+0.5, +1 m, then decreases when SLR=+2 m, and finally increases when SLR=+5 m. In our study, the M2 amplitude decreases for SLR=+0.5, +1 m, and +2 m, and increases for SLR=+5 m. Our results are consistent with those of Pelling et al. (2013) for SLR=+2 m and +5 m, but not with those of Pelling and Green (2014) for smaller SLRs. As our results are consistent with the results of Pelling et al. (2013) and Pelling and Green (2014) for the "no flood" case, we suspect that the observed differences relate to the topographic data used in the various studies: Pelling and Green (2014) used GEBCO data with a resolution of 1 arc-minute, whereas we used GTOPO30 data with a resolution of 0.5 arc-minute. Regardless of the explanation for these differences, as shown by the above results, over a very large SLR range (from +0.5 to +5 m), the sign of the M2 component changes depending on the SLR value in the Irish Sea. Our study confirms this spatial dissimilarity of the M2 component, but shows that, for SLR≤2 m, the change in high tide levels remains spatially similar over a large part of the Irish Sea, regardless of the flooding option. Lastly, our conclusion that the changes are less proportional to SLR for "flood" cases than for "no flood" cases is in agreement with the results of Pelling et al. (2013) and Pelling and Green (2014).

In the above coastal defense scenarios, we assumed a spatially uniform choice ("no flood" or "flood"). In reality, this will not be uniform. Pelling and Green (2014) investigated the effect of partial flooding. This third scenario causes the greatest changes in M2 amplitude. This result confirms that information on future tides requires knowledge of future choices. It also shows that coastal defense strategies have a cross-border dimension. One way to reduce uncertainties in terms of water level projections would be to establish direct

Table 1
Summary of recent studies (after 2012) showing the methods used. 2DH refers to a depth-averaged 2D model. For a review of earlier modelling studies, see Pickering et al. (2012).

Study	Method Description Model; Domain; grid size; open boundary condition; Astronomical Potential; land conditions; SLR scenario; Result analyzed (duration, variable)
Pickering et al. (2012)	DCSMv5 (2DH); northwestern European Shelf; 1/12° x 1/8° (8×8 km); [M2; M2, S2, N2, K2, NU2, L2, K1, O1, P1, Q1]; no astronomical potential; no flood; [0, 2, 10] m; ([5 days; 25 days], [M2 for grid analysis, water level for port analysis])
Ward et al. (2012)	KUTM (2DH); northwestern European Shelf; 1/12°; water level and currents from TPXO.6; astronomical potential (M2, S2, N2, K1, O1); flood; [0:1:5] m; (30 days, M2 & M4)
Pelling et al. (2013)	KUTM (2DH); northwestern European Shelf; 1/12°; water level and currents from TPXO; astronomical potential (M2, S2, N2, K1, O1); [flood; no flood]; [0, 2:0.5:5] m; (30 days, M2)
Pelling and Green (2014)	OTIS (2DH); northwestern European Shelf; 1/60°; water level from TPXO7.2; no information on astronomical potential; [flood; no flood; flood defense scheme]; [0:0.25:1] m; (3 days, M2)
This study	MARS (2DH); northwestern European Shelf; 1/55° x 1/34° (2×2 km); predicted tide from FES2004; no astronomical potential; [no flood; flood]; [−0.25–10 m]; (1 year, maximum/minimum water level, O1, K1, N2, M2, S2, K2, 2N2, M4, MS4, MN4)

interactions between modelling (by integrating SLR, tides, atmospheric surges, and waves), extreme statistics on water levels, and coastal managers at local, national, and cross-national scales.

5.4. Flooding implications

The majority of tide gauges along the world's coastlines show changes in extreme water levels which are comparable to the rising mean sea-level (MSL) (Woodworth et al., 2011). Future total water levels will result from the sum of relative SLR, which includes vertical ground motions in a terrestrial framework (Nicholls et al., 2014), tide, surge and interaction components. Sea-level rise will induce changes in tidal water levels (locally up to 15% of SLR), as well as storm surges, whether directly or indirectly through tide-surge interactions (this interaction can reach tens of centimeters, as shown by Idier et al., 2012). In addition to the effects of SLR-induced tidal changes on water levels in the German Bight, Arns et al. (2015) showed that increases in design water levels are expected to be above the SLR rate, an assertion also supported by our study on this area. Importantly, the difference in heights of extreme water levels for events with return periods of 100 years to 1000 years is generally not larger than several 10's of centimeters. Hence, a 10–15% modulation of SLR by the SLR-tide interaction process is not negligible from the point of view of flood prevention and adaptation planning. In fact, all other things being equal, some areas such as the western English Channel will have more time to adapt before critical levels are exceeded. Conversely, other locations such as the German Bight ("no flood" case) will require adaptation measures earlier. For the numerous locations where the high tide level (ξ_{max}) varies proportionally to sea-level rise, the values obtained in Figs. 6b2, 11b1 and b2 can be used to adjust scenarios for the local extreme water levels that could occur in the future.

The design of future local mean sea-level scenarios is of great importance for coastal adaptation, risk prevention and land use policies. Some countries, such as France, use nationally uniform SLR scenarios. Here, we provide further evidence that this type of approach induces local errors, and that future sea-level scenarios need to be designed regionally and even locally.

6. Conclusions

A validated shallow-water hydrodynamic model has been used to investigate the effects of SLR on the tides of the western European Continental Shelf for a wide range of SLR values (from −0.25 to +10 m). The results show changes in the M2 amplitudes that can reach values of +/−15% of SLR, confirming recent studies. Moreover, the 12 largest astronomic tidal components, as well as the maximum water levels, have been investigated. The largest changes in amplitude were observed for the M2, S2, N2, M4 and MS4 tide components. The changes in tidal water levels appear to be not exactly similar to the changes in M2 components, highlighting the need to take into account other tidal components, especially the quarter-diurnal ones, to accurately anticipate future SLR-tide interactions. In terms of spatial similarity and proportionality (question Q1), when it is assumed that land areas are protected from flooding, the tide components and the maximum tidal water levels vary proportionally to SLR over most of the domain, up to at least SLR=+2 m. However, some areas show non-proportional behavior (e.g., the Celtic Sea and the German Bight). The changes in high tide water levels range from −15% to +15% of SLR, with a decrease observed in the western English Channel and increases in the Irish Sea, the southern part of the North Sea and the German Bight. The changes in tidal water levels result from the competition between reduced bed friction, changes in wave characteristics (and resonance properties), and increased reflection at the coast, i.e., between local and non-local processes (question Q2).

The tide in the eastern part of the North Sea and the Celtic Sea is very sensitive to the "flood"/"no flood" option (question Q3), while the tide in the northern channel of the Irish Sea and in the western English Channel is almost insensitive. In addition, the tidal changes relative to local SLR values induced by non-uniform SLR display significant differences over 8% of the domain (mainly in areas exhibiting a non-proportional response to uniform SLR). Thus, the results from studies assuming uniform SLR, although valid for investigating the mechanisms responsible for SLR-induced changes, should be used with caution, especially in areas exhibiting a non-proportional response to SLR, such as the Celtic Sea or the German Bight (question Q4).

With the implementation of the first coastal adaptation plans, it is becoming important to better anticipate future changes in tidal dynamics and total water levels in the context of future regional SLR. The main trends in SLR-tide interactions can be relatively well anticipated in many areas of the western European continental shelf. Advances in knowledge of future (non-uniform) sea-level rise, coastal defense choices, geormorphological changes and coastal ground motion should allow further reductions in the uncertainty of predictions.

Acknowledgements

The present study was funded by BRGM (PDR15DRP21) (as an internal CCRA project). The authors wish to thank IFREMER for permission to use the MARS code, LEGOS (Damien Allain) for providing the Tidal Toolbox software, SHOM for the tide predictions (SHOMAR application) and for the shallow-water bathymetric data, BODC for the deep-water bathymetric data (GEBCO) and the USGS for the topographic data (GTOPO30). The authors are grateful to C. Oliveros, L. Pineau-Guillou and X. Bertin for fruitful discussions, as well as to the reviewers for their remarks and recommendations.

References

Arns, A., Wahl, T., Dangendorf, S., Jensena, J., 2015. The impact of sea level rise on storm surge water levels in the northern part of the German Bight. Coast. Eng. 96, 118–131.

Bertin, X., Bruneau, N., Breilh, J.F., Fortunato, A.B., Karpytchev, M., 2012. Importance of wave age and resonance in storm surges: the case Xynthia, Bay of Biscay. Ocean Model. 42, 16–30.

Church, J., Clark, P., Cazenave, A., Gregory, J., Jevrejeva, S., Merrifield, M., Milne, G., Nerem, R., Nunn, P., Payne, A., Pfeffer, W., Stammer, D., Unnikrishnan, A.S., 2013a. Sea Level Change, pages 1137–1216. Climate Change 2013: The Physical Science Basis. Contribution of Working Group I to the Fifth Assessment Report of the Intergovernmental Panel on Climate Change. Cambridge University Press, Cambridge, United Kingdom and New York, NY, USA.

Church, J.A., Clark, P.U., Cazenave, A., Gregory, J.M., Jevrejeva, S., Levermann, A., Merrifield, M.A., Milne, G.A., Nerem, R.S., Nunn, P.D., Payne, A., Pfeffer, W., Stammer, D., Unnikrishnan, A.S., 2013b. Sea-level rise by 2100. Science 342 (6165), (1445–1445).

Church, J.A., White, N.J., 2011. Sea-level rise from the late 19th to the early 21st century. Surv. Geophys. 32 (4–5), 585–602.

Clark, P.U., Shakun, J.D., Marcott, S.A., Mix, A.C., Eby, M., Kulp, S., Levermann, A., Milne, G.A., Pfister, P.L., Santer, B.D., Schrag, D.P., Solomon, S., Stocker, T.F., Strauss, B.H., Weaver, A.J., Winkelmann, R., Archer, D., Bard, E., Goldner, A., Lambeck, K., Pierrehumbert, R.T., Plattner, G.-K., 2016. Consequences of twenty-first-century policy for multi-millennial climate and sea-level change. Nat. Clim. Change 6, 360–369.

de Ronde, J.G., 1989. Past and Future sea level rise in the Netherlands in Workshop on Sea Level Rise and Coastal Processes, Palm Beach, Florida, 9–11March 1988. US Department of Energy Report DOE/NBB-0086, Washington,DC, 253–280.

Gerritsen, H., de Fries, H., Philippart, M., 1995. The Dutch continental shelf model. Coast. Estuar. Stud. 47, 425–467.

Green, J.A.M., 2010. Ocean tides and resonance. Ocean Dyn. 60 (1243), 1253.

Hay, C.C., Morrow, E., Kopp, R.E., Mitrovica, J.X., 2015. Probabilistic reanalysis of twentieth-century sea-level rise. Nature.

Hinkel J., Lincke D., Vafeidis A.T., Perrette M., Nicholls R.J., Tol R.S.J., Marzeion B., Fettweis X., Ionescu C., Levermann A., 2013. Coastal flood damage and adaptation costs under 21st century sea-level rise PNAS 2014, doi:http://dx.doi.org/10.1073/pnas.1222469111.

Howarth M.J.,1990. Atlas of tidal elevations and currents around the British Isles. Department of Energy, Offshore Technology Report, OTH89293, appendix & charts, 16pp.

Idier, D., Dumas, F., Muller, H., 2012. Tide-surge interaction in the English Channel. Nat. Hazards Earth Syst. Sci. 12, 3709–3718.

Idier, D., van der Veen, H., Hulscher, S.J.M.H., 2009. Grain Size and sand bank modelling. J. Geophys. Res. – Earth Surf.. http://dx.doi.org/10.1029/2008JF001140.

Jevrejeva, S., Grinsted, A., Moore, J.C., 2014. Upper limit for sea level projections by 2100. Environ. Res. Lett. 9 (10), 104008.
Kopp, R.E., Horton, R.M., Little, C.M., Mitrovica, J.X., Oppenheimer, M., Rasmussen, D.J., Strauss, B.H., Tebaldi, C., 2014. Probabilistic 21st and 22nd century sea-level projections at a global network of tide-gauge sites. Earth's. Future 2, 383–406. http://dx.doi.org/10.1002/2014EF000239.
Lazure, P., Dumas, F., 2008. An external-internal mode coupling for a 3D hydrodynamical model for applications at regional scale (MARS). Adv. Water Resour. 31, 233–250.
Le Cozannet, G., Garcin, M., Yates, M., Idier, D., Meyssignac, B., 2014. Approaches to evaluate the recent impacts of sea-level rise on shoreline changes. Earth-Sci. Rev. 138, 47–60.
Liang, D., Xia, J., Falconer, R.A., Zhang, J., 2014. Study on tidal resonance in Severn Estuary and Bristol Channel. Coast. Eng. J. 56, 01.
Lyard, F., Lefèvre, F., Letellier, T., Francis, O., 2006. Modelling the global ocean tides: modern insights from FES2004. Ocean Dyn.. http://dx.doi.org/10.1007/s10236-006-0086-x.
Mawdsley, R.J., Haigh, I.D., Wells, N.C., 2015. Global secular changes in different tidal high water, low water and range levels. Earth's. Future 3, 66–81. http://dx.doi.org/10.1002/2014EF000282.
Mitrovica, J.X., Hay, C.C., Morrow, E., Kopp, R.E., Dumberry, M., Stanley, S., 2015. Reconciling past changes in Earth's rotation with 20th century global sea-level rise: resolving Munk's enigma. Sci. Adv. 1, e1500679.
Nicholls, R.J., Hanson, S.E., Lowe, J.A., Warrick, R.A., Lu, X., Long, A.J., 2014. Sea-level scenarios for evaluating coastal impacts. Wiley Interdiscip. Rev.: Clim. Change 5 (1), 129–150.
Parker, B.B., 2007. Tidal Analysis and Prediction (PhD thesis). NOAA Special Publication NOS CO-OPS 3, (Library of Congress Control Number: 2007925298).
Pelling, H.E., Green, J.A.M., Ward, S.L., 2013. Modelling tides and sea-level rise: to flood or not to flood. Ocean Model. 63, 21–29.
Pelling, H.E., Green, J.A.M., 2014. Impact of flood defences and sea-level rise on the European Shelf tidal regime. Cont. Shelf Res. 85, 96–105.
Pickering, M.D., Wells, N.C., Horsburgh, K.J., Green, J.A.M., 2012. The impact of future sea-level rise on the European Shelf tides. Cont. Shelf Res. 35, 1–15.
Pugh, D.J., 1987. Tides, Surges and Mean Sea-level. A Handbook for Engineers and Scientists. Wiley, Chichester, 472.
Ranasinghe, R., Callaghan, D., Stive, M.J.F., 2012. Estimating coastal recession due to sea level rise: beyond the Bruun rule. Clim. Change 110 (3–4), 561–574.
Roos, P.C., Velema, J.J., Hulscher, S.J.M.H., Stolk, A., 2011. An idealized model of tidal dynamics in the North Sea: resonance properties and response to large-scale changes. Ocean Dyn. 61, 2019–2035. http://dx.doi.org/10.1007/s10236-011-0456-x.
Slangen, A.B.A., Carson, M., Katsman, C.A., van de Wal, R.S.W., Köhl, A., Vermeersen, L.L.A., Stammer, D., 2014. Projecting twenty-first century regional sea-level changes. Clim. Change 124 (1–2), 317–332.
Stive, M.J.F., Aarninkhof, S.G.J., Hamm, L., Hanson, H., Larson, M., Wijnberg, K.M., Nicholls, R.J., Capobianco, M., 2002. Variability of shore and shoreline evolution. Coast. Eng. 47 (2), 211–235.
Ward, S.L., Green, J.A.M., Pelling, H.E., 2012. Tides, sea-level rise and tidal power extraction on the European shelf. Ocean Dyn. 62, 1153–1167.
Weisse, R., von Storch, H., Niemeyer, H.D., Knaack, H., 2012. Changing North Sea storm surge climate: an increasing hazard? Ocean Coast. Manag. 68, 58–68.
Winkelmann, R., Levermann, A., Ridgwell, A., Caldeira, K., 2015. Combustion of available fossil fuel resources sufficient to eliminate the Antarctic Ice Sheet. Sci. Adv. 1 (8). http://dx.doi.org/10.1126/sciadv.1500589.
Wong, P.P., Losada, I.J., Gattuso, J.-P., Hinkel, J., Khattabi, A., McInnes, K.L., Saito, Y., Sallenger, A., 2014. Coastal systems and low-lying areas. In: Field, C.B., Barros, V.R., Dokken, D.J., Mach, K.J., Mastrandrea, M.D., Bilir, T.E., Chatterjee, M., Ebi, K.L., Estrada, Y.O., Genova, R.C., Girma, B., Kissel, E.S., Levy, A.N., MacCracken, S., Mastrandrea, P.R., White, L.L. (Eds.), Climate Change 2014: Impacts, Adaptation, and Vulnerability. Part A: Global and Sectoral Aspects. Contribution of Working Group II to the Fifth Assessment Report of the Intergovernmental Panel on Climate Change. Cambridge University Press, Cambridge, United Kingdom and New York, NY, USA, 361–409.
Woodworth, P.L., 2010. A survey of recent changes in the main components of the ocean tide. Cont. Shelf Res. 30, 1680–1691.
Woodworth, P.L., Menéndez, M., Gehrels, W.R., 2011. Evidence for century-timescale acceleration in mean sea levels and for recent changes in extreme sea levels. Surv. Geophys. 32 (4–5), 603–618. http://dx.doi.org/10.1007/s10712-011-9112-8.
Wöppelmann, G., Marcos, M., Santamaría-Gómez, A., Martín-Míguez, B., Bouin, M.N., Gravelle, M., 2014. Evidence for a differential sea level rise between hemispheres over the twentieth century. Geophys. Res. Lett. 41 (5), 1639–1643.

Further reading

Pingree, R.D., Griffiths, D.K., Maddock, L., 1984. Quarter diurnal shelf resonances and tidal bed stress in the English Channel. Cont. Shelf Res. 3 (3), 267–289.